

Equal Incremental Cost-Based Optimization Method to Enhance Efficiency for IPOP-Type Converters

Hanfeng Cai, Haiyang Liu, Heyang Sun, and Qiao Wang

Abstract—Systematic optimization over a wide power range is often achieved through the combination of modules of different power levels. This paper addresses the issue of enhancing the efficiency of a multiple module system connected in parallel during operation and proposes an algorithm based on equal incremental cost for dynamic load allocation. Initially, a polynomial fitting technique is employed to fit efficiency test points for individual modules. Subsequently, the equal incremental cost-based optimization is utilized to formulate an efficiency optimization and allocation scheme for the multi-module system. A simulated annealing algorithm is applied to determine the optimal power output strategy for each module at given total power flow requirement. Finally, a dual active bridge (DAB) experimental prototype with two input-parallel-output-parallel (IPOP) configurations is constructed to validate the effectiveness of the proposed strategy. Experimental results demonstrate that under the 800W operating condition, the approach in this paper achieves an efficiency improvement of over 0.74% by comparison with equal power sharing between both modules.

Index Terms—Equal Incremental Cost, Efficiency Optimization, Load Distribution, IPOP-Connected DC-DC Converters, Dual Active Bridge (DAB).

I. INTRODUCTION

IN this day and age, electric vehicles (EVs) [1] have become a rapidly-expanding competitor to traditional fuel cars due to their sustainability, cost-effectiveness, and reduced noise. In 2030, the market share of EVs is predicted to grow by 30% [2], which leads to the demand of more reliable, higher power density, and low cost power electronic solutions [3]. Currently, there exists proposed charging infrastructure like single stage vehicle on-board chargers (OBCs) [4] and two stage AC-DC and DC-DC converter [5]. As the global automotive industry shifts towards electric vehicles, it becomes crucial to develop ways to improve the efficiency of power converters to accommodate the diverse power and voltage requirements of different vehicles.

Systematic solutions like adaptive charging [6] and iteration-based algorithm [7] have been proposed for EV charging applications. Different modulation or control strategies have been experimented [8] [9] [10] to enhance efficiency, and numerous topologies like soft-switching buck-boost [11] and multi-phase multi-voltage converters [12] are presented. Still, one of the most effective solutions is DC-DC converters, such as Dual-Active Bridges (DAB) [13]–[16], which support bidirectional power transfer, galvanic isolation, high power density, and current-stress minimization techniques like triple-phase shift (TPS) control [17].

However, increased power requirement and physical limitations requires innovations on converters. One of them is three-phase converters [18], [19]. Another proposed design utilizes input-serial-output-parallel (ISOP) configuration to improve efficiency for smart transformer applications [20]. To further enhance design redundancy [21] and accommodate a wider range of power requirement [22], Input-parallel-output-parallel (IPOP)-connected converters offer a simple solution using independent modular control [23]. Multiple converter systems are able to achieve high power rating with lower powered converters through power sharing [24]. In contrast, a single module is often optimized for a power level and is unable to adjust across dynamic power requirements due to physical limitations. While some existing literature utilizes phase-shift control [25], soft-switching [26], and current sharing techniques [27]. For optimization on light load conditions, dynamic active phase variation with load demand has been proposed [28]. Another paper presents a passive current sharing method based first-order digital sine filter [29]. This article uniquely provides a algorithmic way to calculate the optimal operating conditions for each module based on their power profiles.

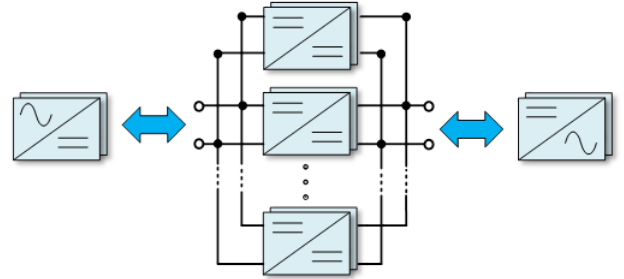


Fig. 1: Schematic diagram for IPOP-connected converter modules.

This article is organized as follows: Section II identifies the key problems of optimizing multiple IPOP-connected converters, Section III showcases the solutions in four steps: A curve-fitting approach for efficiency analysis, followed by priority list (PL) method and equal incremental cost-based approach, and ended by an application of the simulated-annealing algorithm for systematic computation. Section IV illustrates the modulation strategy of the IPOP-connected DABs. Lastly, the experimental results are laid out in Section V.

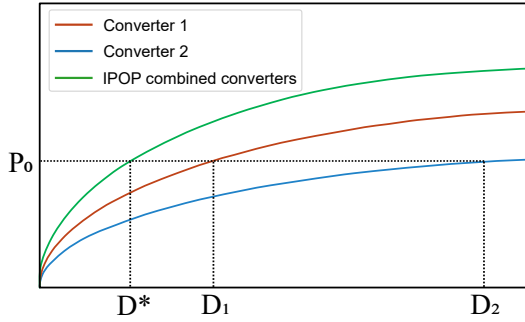


Fig. 2: Power output and duty cycle relationship for non-identical modules.

II. PROBLEM DESCRIPTION

It is common to use multiple modules connected in an IPOPOP configuration, as illustrated in Fig. 1. In this connection scheme, fully identical modules are typically used to simplify the system's design. Currently, for the optimization of the optimal configuration of identical DC converter sub-modules, two identical IPOPOP-connected-DAB converters have been proposed [22], where equal power sharing results in the highest efficiency.

However, to achieve specific functionalities or operational characteristics, it is also common to use sub-modules with different parameters or topologies [30]. This IPOPOP configuration with non-identical sub-modules brings more flexibility to the system's control strategy, but at the same time, increasing the complexity in system design, such as cost, efficiency, and current stress. This paper primarily focuses on the efficiency optimization problem for such non-identical sub-module IPOPOP topologies.

As shown in Fig. 2, the red and blue lines represent the output power and duty cycle for two different types of non-identical modules, respectively. The green line represents the combined power output when both modules are active. It can be observed that there exists a certain algebraic relationship between power transfer and duty. Under the condition of the same output power, the two different types of modules in the IPOPOP configuration have different duty cycles. Given a fixed output power (P_0), and the IPOPOP-configured modules operate with a duty cycle of D^* , the duty cycle for the red curve (converter 1) is D_1 , and the duty cycle for the blue curve (converter 2) to achieve the same P_0 power output is D_2 .

Fig. 3 illustrates the relationship between duty cycle and efficiency. It can be observed that under the mentioned duty cycle conditions, the IPOPOP-connected modules operate at a lower efficiency compared to the cases where the two types of modules are running independently, specifically at the duty cycle D^* .

At light load conditions, converter 2 running independently achieves higher efficiency. In the mid-range power output region, converter 1 exhibits higher overall efficiency compared to the other two configurations. However, under high power output conditions, the IPOPOP configuration with both types of modules achieves the highest overall efficiency, significantly surpassing the other two configurations.

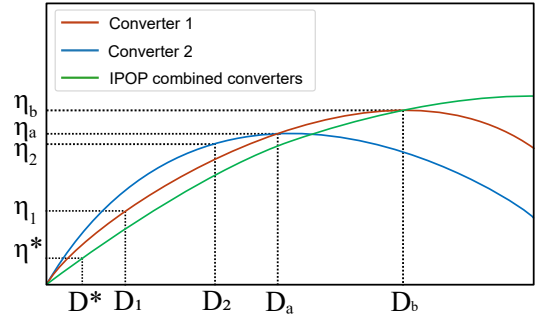


Fig. 3: Efficiency versus duty cycle for IPOPOP-connected modules.

In summary, it can be concluded that the efficiency performance of different module configurations varies in different power ranges. As shown in Fig. 3, before the operating point D_a , the blue curve (converter 2) exhibits the highest efficiency, while the IPOPOP configuration with non-identical modules (green curve) shows the lowest. When the duty cycle exceeds D_a , the red curve (converter 1) demonstrates significantly higher efficiency compared to the other two modes. When the duty cycle exceeds D_b , the efficiency of module 1 and module 2 operating together is higher.

It is possible to optimize the operation of different modules at their respective optimal output power points based on these characteristics. The IPOPOP topology with non-identical modules can achieve higher efficiency under high power load conditions. Under light load conditions, each of the two modules can operate on their own efficiency-optimized operating regions, thereby optimizing the combined power converter modules.

Based on the mentioned problem, the objective function for the efficiency optimization problem of the IPOPOP topology with non-identical modules can be summarized as follows:

$$\begin{cases} \max(\eta) = \frac{P_{out}}{P_{in}} \\ P_{out} = \sum_{i=1}^m P_i(I_i) \end{cases} \quad (1)$$

The main objective of this study is to maximize the overall efficiency (η) by optimizing power allocation. The total output power is calculated as the sum of the output powers of each module, which is a function of their respective duty cycles. The proposed solution must satisfy the constraint that each module must operate within its own power range.

This paper introduces a systematic algorithm to calculate the most efficient load distribution scheme, utilizing the given converter's power-current profile. To validate the effectiveness of this algorithm, experiments were conducted using collected data from two different DABs. The Triple Phase Shift (TPS) modulation strategy is employed to minimize current stress under unidirectional power flow, a usual scenario in EV charging applications. Finally, a comprehensive analysis of the system's dynamic characteristics is conducted. The primary objective of this study is to propose an optimized power allocation approach that ensures the highest overall system efficiency while accounting for power range constraints

associated with each module. The validity of the proposed algorithm is established through experimentation involving two modules, showcasing a significant enhancement over the conventional approach of equal power distribution among all modules.

III. PROBLEM SOLUTION

A. Polynomial fitting of efficiency curves

Current models on converter losses [31], [32] are able to approximate DC-DC converters with numerous non-idealities, such as copper loss, leakage inductance, eddy current, and hysteresis, etc. The conversion efficiency η can be modeled using the quadratic loss model [33]:

$$\eta = \frac{P_{out}}{P_{in}} = \frac{P_{out}}{P_{out} + P_{loss}} = \frac{P_{out}}{a_2 \cdot P_{out}^2 + (a_1 + 1) \cdot P_{out} + a_0} \quad (2)$$

The linear term models the switching loss as a function of I_{out} , the quadratic term originates from MOSFETS's resistance loss proportional to I_{out}^2 , and the constant term models auxiliary circuits. However, non-linear and high-order losses like switching loss are much harder to model. This article, hence, adopts a curve-fitting approach to approximate the input/output power relationship experimentally.

The input and output power can be modeled as N^{th} degree polynomials with respect to current:

$$p_{U_1}(I) = a_N I^N + a_{N-1} I^{N-1} + \dots + a_2 I + a_1 \quad (3)$$

$$p_{U_2}(I) = b_N I^N + b_{N-1} I^{N-1} + \dots + b_2 I + b_1 \quad (4)$$

Coefficients $\{a_N, a_{N-1}, \dots, a_1\}$ and $\{b_N, b_{N-1}, \dots, b_1\}$ can be computed via curve-fitting algorithms. It is worth noted that N is at least 3 given $P_{out} = I^2 R$ to model additional losses, and a higher degree of curve fitting can yield better accuracy in modeling additional high-order non-idealities.

B. Priority assignment to each converter

The problem of determining the maximum efficiency, which module should operate, and the output power of each designated module belongs to the NP-completeness category: There are no existing polynomial-time algorithms but exhaustive methods. However, given different converters of the same topology but various power ratings, higher-rated power modules are typically less efficient due to their higher operating temperature [34] and core loss. Thus, the Priority List (PL) method can be adopted in this case to allocate priority to each converter by arranging each module by their maximum efficiency. Known the expression of $P_{out} = f(P_{in})$, developing an order of the maximum efficiency η of each module from greatest to least determines the sequence of which each module should be powered. Each converter will, therefore, join the operation in the order given by the priority queue.

C. Mathematical modeling of N IPOP-connected converters

With the priority order list computed, the switching point between two operating modes can be determined using equal-incremental cost method. thereby obtaining the optimal combination of modules based on a power output requirement.

1) *Intersection point solution:* One combination of m converters has the overall efficiency modeled as a function of their individual input and output power relative to their respective current:

$$\eta = \frac{P_{out}(I_1) + P_{out}(I_2) + \dots + P_{out}(I_m)}{P_{in}(I_1) + P_{in}(I_2) + \dots + P_{in}(I_m)} \quad (5)$$

We can apply Lagrange Multiplier with respect to individual currents.

$$\frac{\partial \eta}{\partial I_1} = \frac{\frac{dP_{out}(I_1)}{dI_1} \sum_{i=1}^m P_{in}(I_i) - \frac{dP_{in}(I_1)}{dI_1} \sum_{i=1}^m P_{out}(I_i)}{(\sum_{i=1}^m P_{in}(I_i))^2} \quad (6)$$

$$\frac{\partial \eta}{\partial I_2} = \frac{\frac{dP_{out}(I_2)}{dI_2} \sum_{i=1}^m P_{in}(I_i) - \frac{dP_{in}(I_2)}{dI_2} \sum_{i=1}^m P_{out}(I_i)}{(\sum_{i=1}^m P_{in}(I_i))^2} \quad (7)$$

⋮

$$\frac{\partial \eta}{\partial I_m} = \frac{\frac{dP_{out}(I_m)}{dI_m} \sum_{i=1}^m P_{in}(I_m) - \frac{dP_{in}(I_m)}{dI_m} \sum_{i=1}^m P_{out}(I_m)}{(\sum_{i=1}^m P_{in}(I_i))^2} \quad (8)$$

At maximum efficiency, all partial derivatives equate to 0. For the j^{th} module:

$$\frac{dP_{out}(I_j)}{dI_j} \sum_{i=1}^m P_{in}(I_m) = \frac{dP_{in}(I_j)}{dI_j} \sum_{i=1}^m P_{out}(I_m) \quad (9)$$

Divide any two equations to cancel common terms:

$$\frac{dP_{out}(I_1)}{dP_{in}(I_1)} = \frac{dP_{out}(I_2)}{dP_{in}(I_2)} = \dots = \frac{dP_{out}(I_m)}{dP_{in}(I_m)} \quad (10)$$

Hence, as another module joins the operation after switching, equation (9) can be applied to $m + 1$ modules.

$$\frac{dP_{out}(I'_1)}{dP_{in}(I'_1)} = \frac{dP_{out}(I'_2)}{dP_{in}(I'_2)} = \dots = \frac{dP_{out}(I'_{m+1})}{dP_{in}(I'_{m+1})} \quad (11)$$

Meanwhile, the total input (12) and output (13) power are the same for the two combinations at the switching point.

$$\sum_{i=1}^m P_{in}(I_i) = \sum_{i=1}^{m+1} P_{in}(I'_i) \quad (12)$$

$$\sum_{i=1}^m P_{out}(I_i) = \sum_{i=1}^{m+1} P_{out}(I'_i) \quad (13)$$

Solving equation (10) to (13) yields the input and output power of each module at the intersection point. If a solution is not within the minimum and maximum loads requirement: $P_{out,min}(I_i) \leq P_{out}(I_i) \leq P_{out,max}(I_i)$, according to Karush–Kuhn–Tucker conditions (KKT), the module should be operating at its boundary condition. The load distribution of the remaining modules should be recalculated via equation (10) - (13) by removing the modules operating at the boundary condition from the total output power. Additionally, from equation (10), it can be noted that identical power converter modules always operate at the same output power, which reduces the algorithm complexity.

2) Optimal solutions to dynamic power requirements:

Using the Lagrange Multiplier method to solve for $P_{in}(I_i)$ and $P_{out}(I_i)$ for each individual converter requires solving $2m + 1$ equations, where there are m different modules available, thus, can be complex for dynamic load adjustment. Additionally, when modules are operating at their boundary conditions, the above-mentioned equations have to be solved repeatedly. Dynamic optimization algorithms are good candidates for such problems. This article employs the Simulated Annealing Algorithm due to its ability to escape local minimums by generating perturbations on a solution. As the perturbation temperature decreases, the system effectively converges to a globally optimized efficiency. By incorporating the switching point coordinates identified in the preceding section, the optimal solution can be determined by the following algorithm:

- i) Define initial temperature $T = T_0$, and the output power of each module is randomly defined based on the given total output power. Obtain the current total efficiency.
- ii) Calculate the temperature $T = kT$ for the next period. k ($0 < k < 1$) is the rate of temperature decrease (cooling).
- iii) Based on the solution obtained, generate a new solution by random disturbance, and the corresponding change in efficiency $\Delta\eta$. If $\Delta\eta > 0$, the new solution is accepted as the optimal solution. Otherwise, Metropolis–Hastings algorithm determines whether to accept the solution by the probability $P = e^{\frac{\Delta\eta}{kT}}$.
- iv) At the current temperature, iterate step 3 by l times.
- v) If the temperature has reached the accepted threshold temperature T_{thres} , then the current solutions are considered optimal. Otherwise, return to step 2.

3) *Overall logic diagram:* Therefore, a systematic approach is developed to decide the combination and operating conditions of power converters at maximum overall efficiency. First, a priority queue is computed by sorting the efficiency of each module from greatest to least. Then, the intersection point is computed via the Lagrange Multiplier, which determines the point of switching from one combination to another and the optimal combination between two switching points. Finally, the Simulated Annealing Algorithm decides the optimal solutions to any dynamic output power requirements. Therefore, the method proposed by this paper can be summarized by flow chart Fig. 4.

IV. SYSTEM MODELING

There are generally four efficiency improvement techniques for DABs: Optimization based on power loss model [36], non-active power optimization [37], zero-voltage-switching range optimization [38], and inductor current optimization [39]. For a DAB converter, the switching frequency is often restricted due to the physical size and output ripple requirement, therefore cannot be easily changed. However, copper loss, core loss, switching loss, and lumped resistance are functions of the inductor current, making current stress minimization the most effective solution.

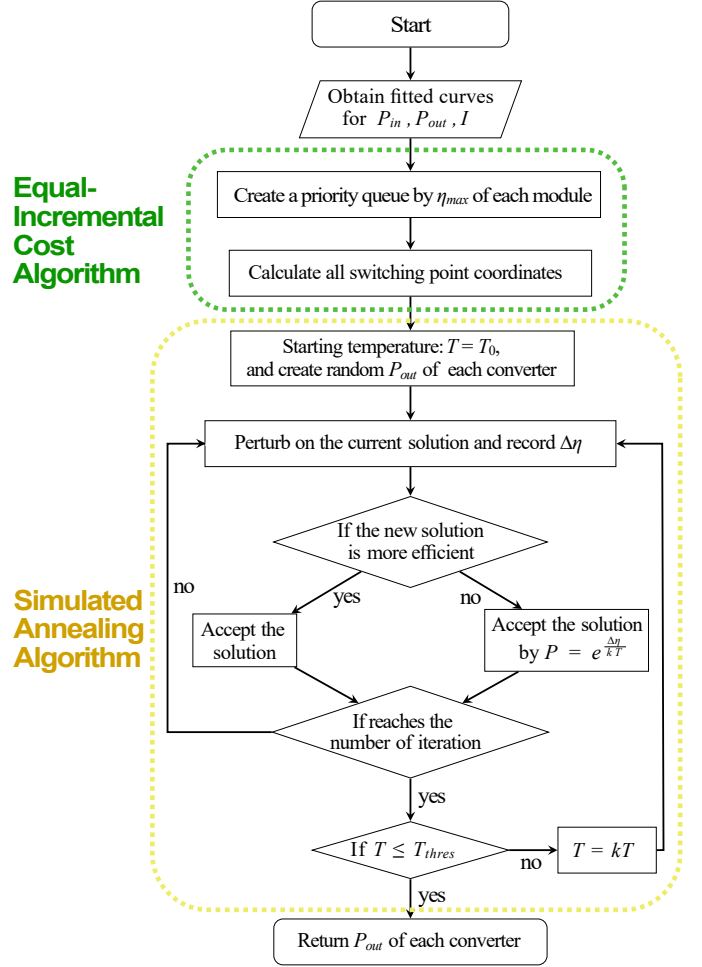


Fig. 4: Algorithm flow chart diagram, which determines the optimal converter operating combination and power.

The average output power of a DAB can be modeled as

$$P_{avg} = \frac{1}{T} \int_{t_0}^{t_0+T} u_l(t) i_l(t) dt \quad (14)$$

where T is the switching period, and $u_l(t)$ and $i_l(t)$ are the voltage and current on the inductor, which can be controlled by phase shift ratios D_1 , D_2 , and D_3 , where D_1 is the primary inner phase shift ratio, D_2 is the outer phase shift ratio, and D_3 is the secondary inner phase shift ratio. Current phase-shift control method like single-phase-shift (SPS) modulation [40], where $D_1 = 0$ and $D_2 - D_3 = 0$. However, although SPS control provides certain advantages, it comes with drawbacks such as high circulating power and the absence of Zero Voltage Switching (ZVS) capability. These limitations necessitate the use of higher dimensional modulation techniques [41], such as dual-phase-shift (DPS), extended-phase-shift (EPS), and triple-phase-shift (TPS) that utilizes all three dimensions of control D_1 , D_2 , and D_3 [35], which the experiment will adopt.

For EV charging applications, maximum forward transmission power is desired. Research [17] lays out 12 modes of TPS control, each corresponding to different forward and reverse charging characteristics. This paper focuses on the two modes as illustrated in table I for optimal forward power

TABLE I: Phase shift strategy for minimized current stress under buck and boost modes [35]

Voltage	Range of p	Phase-shift D_1, D_3	Phase-shift D_2	Mode
$k > 1$ Boost	$0 \leq p < \frac{2(k-1)}{k^2}$	$D_1 = 1 - \sqrt{\frac{p}{2(k-1)}}$ $D_3 = 1 - \sqrt{\frac{pk^2}{2(k-1)}}$	$D_2 = \frac{1}{2}(1 + D_1 - D_3 - \sqrt{-D_1^2 - D_3^2 - p + 1})$	2
	$\frac{2(k-1)}{k^2} \leq p \leq 1$	$D_1 = (k-1)\sqrt{\frac{1-p}{k^2 - 2k + 2}}$ $D_3 = 0$	$D_2 = 1 - D_3 - \sqrt{(1-D_1)(1-D_3) - \frac{p}{2}}$	1
$0 < k \leq 1$ Buck	$0 \leq p < 2(k-k^2)$	$D_1 = 1 - \sqrt{\frac{p}{2k(1-k)}}$ $D_3 = 1 - \sqrt{\frac{pk}{2(1-k)}}$	$D_2 = \frac{1}{2}(1 + D_1 - D_3 - \sqrt{-D_1^2 - D_3^2 - p + 1})$	2
	$2(k-k^2) \leq p \leq 1$	$D_1 = 0$ $D_3 = (1-k)\sqrt{\frac{1-p}{2k^2 - 2k + 1}}$	$D_2 = 1 - D_3 - \sqrt{(1-D_1)(1-D_3) - \frac{p}{2}}$	1

transmission with calculated optimal phase-shift values for minimum current stress. Fig. 5 showcases the inductor currents and voltages corresponding to the two modes. Thus, given the inductor voltage during the whole operating range, the current stress (p. u.) can be illustrated as follows:

$$I_m = \begin{cases} -kD_1 + 2D_2 + D_3 + k - 1 & k > 1 \\ -kD_1 + 2kD_2 - D_3(1-2k) + 1 - k & 0 < k \leq 1 \end{cases} \quad (15)$$

$$k = \frac{nU_{in}}{U_{out}} \quad (16)$$

n is the transformer turns ratio, and p is the transmission power in p.u under the condition $0 \leq p \leq 1$.

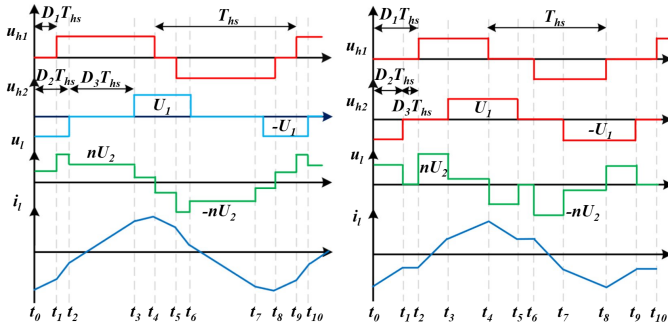


Fig. 5: I/V characteristics of Mode 1 (left) and 2 (right).

V. EXPERIMENTAL RESULT

To validate the effectiveness of the proposed method, two experimental prototypes of DAB modules with different parameters were established, as shown in Fig. 6. Each DAB module consists of eight Insulated Gate Bipolar Transistors (IGBTs) modal No.IGW60T120. The controller adopted for these modules is TMS320F28335. The total leakage inductance of the high-frequency isolation transformer and the sum of auxiliary inductances are $100\mu H$ and $150\mu H$ respectively.

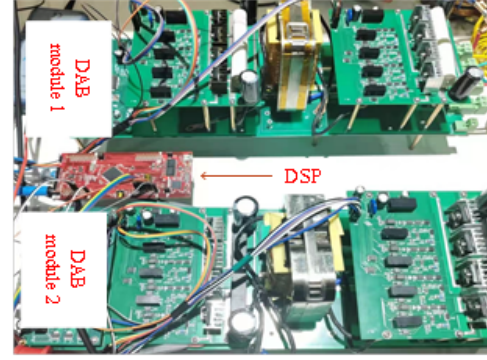


Fig. 6: Experimental Setup for optimizing DAB Load Distribution.

Detailed experimental parameters for the DAB modules are provided in table II in the appendix.

All DAB modules adopt TPS modulation strategy [35] to reduce switching losses and optimize the current stress in each module. As illustrated in the experimental waveform Fig. 7, under the buck operation with a voltage range of 100-80V and a transmission power of 600W, the modulation strategy minimizes the current stress. For Module 1 ($100\mu H$) and Module 2 ($150\mu H$), the waveforms of the high-frequency transformer's voltage and inductor current are shown. This modulation strategy ensures that the inductor current stress is minimized for this specific working condition. By employing the TPS modulation strategy, the DAB module achieves efficient and optimized performance.

To validate the algorithm proposed in this research, power and efficiency data points were collected from two DAB modules. A curve-fitting approach is applied to model the system behavior in all load conditions. As shown in Fig. 8, the module with $150\mu H$ leakage inductance exhibits higher efficiency under light-load conditions, whereas the module with $100\mu H$ leakage inductance performs better at output powers exceeding 290W.

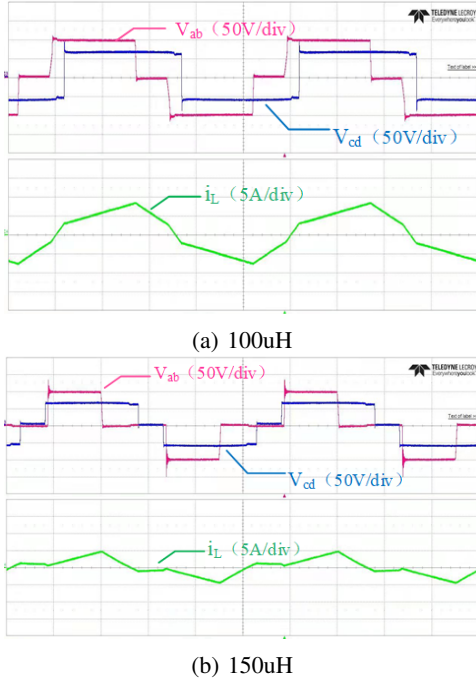


Fig. 7: Voltage and current waveform for optimal current stress for two DABs

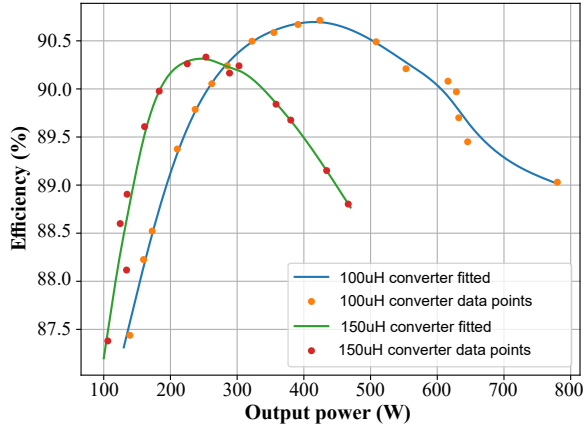


Fig. 8: Experimental data and fitted-fitting result for the two DAB modules

The algorithm developed in this research generates the optimal load distribution scheme, as shown in Fig. 9. The plot illustrates the efficiency of the two DAB modules, and the experimental results closely align with the theoretical expectations. The switching points are identified at $p = 282.75W$ and $p = 549.80W$ according to Equal-Incremental Cost algorithm. In addition, the experiment includes a control group where two modules operate at the same power level for comparison purposes. The experiment's results showcase a substantial increase in efficiency, with improvements of up to 0.74% compared to the even load distribution scheme. This significant enhancement further emphasizes the algorithm's superiority and enables a significantly wider output power range, outperforming individual modules and expanding its applicability across various converter topologies.

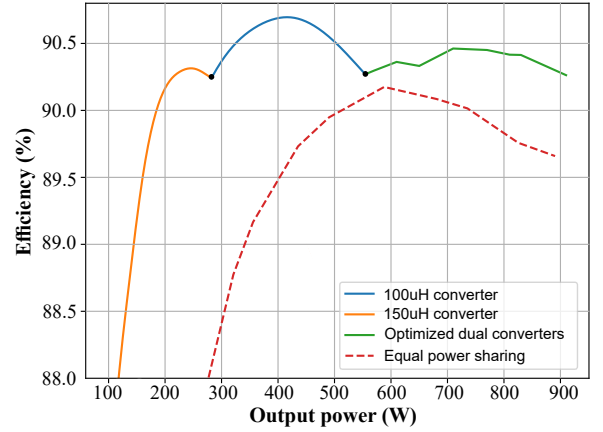


Fig. 9: Overall operating scheme with experiment data and compare group

VI. CONCLUSION

IPOP-connected converters are cost-effective solutions to wide power requirement for EV charging applications. This paper demonstrates that smaller converters can achieve a significant boost in efficiency under the proposed algorithm.

This article proposed a systematic way to compute the operating condition of each module using collected data points. A curve-fitting approach is utilized to define the efficiency curves experimentally. To locate the switching point between two modes in multi-IPOP-connected systems, this study adopts the Equal Incremental Rate method. The system calculations are performed using the Simulated Annealing algorithm to obtain the optimal output distribution scheme for each module under dynamic power requirements. Finally, this study is validated using the two prototype DABs. Experimental results demonstrate that under the operating condition $p = 282.75W$ and $p = 549.80W$, the system should switch from 150uH to 100uH, and 100uH to two modules, when both modules are assigned load distribution according to the Equal Marginal Rate method, a significant efficiency improvement is achieved. By comparison with the two modules operating at the same output power, the proposed algorithm can achieve an increase in efficiency by 0.74%.

APPENDIX

See Table II.

TABLE II: Experiment and simulation parameters

Parameter	Symbol	Value	Unit
Input voltage	U_1	100	V
Output voltage	U_2	80	V
Switching frequency	f_s	10	kHz
Inductance of module 1	Lr_1	100	μH
Inductance of module 2	Lr_2	150	μH
Input capacitance	C_1	320	μF
Output capacitance	C_2	320	μF
MOSFET's gate resistance	R_{gint}	4	Ω
Transformer turns ratio	n	1:1	-

REFERENCES

- [1] M. Ehsani, Y. Gao and A. Emadi, *Modern Electric Hybrid Electric and Fuel Cell Vehicles: Fundamentals Theory and Design*, New York, NY, USA: Taylor & Francis, 2009.
- [2] M. Y. Metwly, M. S. Abdel-Majeed, A. S. Abdel-Khalik, R. A. Hamdy, M. S. Hamad and S. Ahmed, "A review of integrated on-board EV battery chargers: Advanced topologies recent developments and optimal selection of FSCW slot/pole combination", *IEEE Access*, vol. 8, pp. 85216-85242, 2020.
- [3] M. Yilmaz and P. T. Krein, "Review of Battery Charger Topologies, Charging Power Levels, and Infrastructure for Plug-In Electric and Hybrid Vehicles," in *IEEE Transactions on Power Electronics*, vol. 28, no. 5, pp. 2151-2169, May 2013, doi: 10.1109/TPEL.2012.2212917.
- [4] B. Whitaker et al., "A High-Density, High-Efficiency, Isolated On-Board Vehicle Battery Charger Utilizing Silicon Carbide Power Devices," in *IEEE Transactions on Power Electronics*, vol. 29, no. 5, pp. 2606-2617, May 2014, doi: 10.1109/TPEL.2013.2279950.
- [5] Y. -J. Lee, A. Khaligh and A. Emadi, "Advanced Integrated Bidirectional AC/DC and DC/DC Converter for Plug-In Hybrid Electric Vehicles," in *IEEE Transactions on Vehicular Technology*, vol. 58, no. 8, pp. 3970-3980, Oct. 2009, doi: 10.1109/TVT.2009.2028070.
- [6] K. M. Konara and M. L. Kolhe, "Charging coordination of opportunistic EV users at fast charging station with adaptive charging," *2021 IEEE Transportation Electrification Conference (ITEC-India)*, 2021.
- [7] Z. Xie, W. Qi, C. Huang, and H. Li, "Effect analysis of EV optimal charging on DG integration in Distribution Network," *2019 IEEE 8th International Conference on Advanced Power System Automation and Protection (APAP)*, 2019.
- [8] Y. Shi, X.-W. Gui, J. Xi, X. Wang, and X. Yang, "Large power hybrid soft switching mode PWM full bridge DC-DC converter with minimized turn-on and turn-off switching loss," *IEEE Transactions on Power Electronics*, vol. 34, no. 12, pp. 11629-11644, 2019.
- [9] Y.-W. Cho, W.-J. Cha, J.-M. Kwon, and B.-H. Kwon, "High-efficiency bidirectional DAB inverter using a novel hybrid modulation for stand-alone power generating system with low input voltage," *IEEE Transactions on Power Electronics*, vol. 31, no. 6, pp. 4138-4147, 2016.
- [10] B. X. Nguyen, D. M. Vilathgamuwa, G. H. Foo, P. Wang, A. Ong, U. K. Madawala, and T. D. Nguyen, "An efficiency optimization scheme for bidirectional Inductive Power Transfer Systems," *IEEE Transactions on Power Electronics*, vol. 30, no. 11, pp. 6310-6319, 2015.
- [11] M. Pavlovsky, G. Guidi, and A. Kawamura, "Buck/Boost DC-DC converter topology with soft switching in the whole operating region," *IEEE Transactions on Power Electronics*, vol. 29, no. 2, pp. 851-862, 2014.
- [12] G.-J. Su and L. Tang, "A multiphase, modular, bidirectional, triple-voltage DC-DC converter for hybrid and Fuel Cell Vehicle Power Systems," *IEEE Transactions on Power Electronics*, vol. 23, no. 6, pp. 3035-3046, 2008.
- [13] M. Pavlovsky, S. W. H. de Hann and J. A. Ferreira, "Concept of 50kW DC/DC converter based on ZVS quasi -ZCS topology and integrated thermal and electronic design", 2005 European Conference on Power Electronics and Applications, Sept. 2005.
- [14] Rik W. A. A. De Doncker, Deepkraj M. Divan and Mustansir H. Kheraluwala, "A Three-Phase Soft-Switched High-Power-Density dc/dc Converter for High-Power Applications", *IEEE Trans. Industry Applications*, vol. 27, no. 1, pp. 63-73, Jan./Feb. 1991.
- [15] A. KhakparvarYazdi, N. Mazloum, M. MahdaviFard and S. A. Khajehoddin, "Design and Magnetic Optimization of Dual Active Bridge Converters for Energy Storage Application," *2022 IEEE Applied Power Electronics Conference and Exposition (APEC)*, Houston, TX, USA, 2022, pp. 382-389, doi: 10.1109/APEC43599.2022.9773699.
- [16] H. Liu, S. Cui, H. Zhang, Y. Hu, Y. Xue and C. Liu, "The Hybrid Bidirectional DC/DC Converter: Mutual Control and Stability Analysis," in *CSEE Journal of Power and Energy Systems*, vol. 9, no. 2, pp. 769-778, March 2023, doi: 10.17775/CSEEJPES.2021.00260.
- [17] Q. Gu, L. Yuan, J. Nie, J. Sun, and Z. Zhao, "Current stress minimization of dual-active-bridge DC-DC converter within the whole operating range," *IEEE Journal of Emerging and Selected Topics in Power Electronics*, vol. 7, no. 1, pp. 129-142, 2019.
- [18] Z. Li, Y. Wang, L. Shi, J. Huang, Y. Cui and W. Lei, "Generalized averaging modeling and control strategy for three-phase dual-active-bridge DC-DC converters with three control variables", *Proc. IEEE Appl. Power Electron. Conf. Expo.*, pp. 1078-1084, 2017.
- [19] G. Waltrich, M. A. M. Hendrix and J. L. Duarte, "Three-phase bidirectional DC/DC converter with six inverter legs in parallel for EV applications", *IEEE Trans. Ind. Electron.*, vol. 63, no. 3, pp. 1372-1384, Mar. 2016.
- [20] M. Sato et al., "High efficiency design for ISOP converter system with dual active bridge DC-DC converter," *2016 IEEE Applied Power Electronics Conference and Exposition (APEC)*, Long Beach, CA, USA, 2016, pp. 2465-2472, doi: 10.1109/APEC.2016.7468211.
- [21] J.-W. Kim, H.-S. Choi, and B. H. Cho, "A novel droop method for converter parallel operation," *IEEE Transactions on Power Electronics*, vol. 17, no. 1, pp. 25-32, 2002.
- [22] M. Rolak, C. Sobol, M. Malinowski, and S. Stynski, "Efficiency optimization of two dual active bridge converters operating in parallel," *IEEE Transactions on Power Electronics*, vol. 35, no. 6, pp. 6523-6532, 2020.
- [23] T.-T. LE, D. Lee, J. Kim, H.-P. Kieu, and S. Choi, "Modular bidirectional differential converter with series parallel connected output for Ultra-Wide-Voltage Applications: Control, module shedding, and fail-safe operation," *IEEE Transactions on Power Electronics*, vol. 37, no. 1, pp. 617-628, 2022.
- [24] N. Hou, Y. W. Li, and H. Tian, "A reconstructed circuit parameters estimation (RCPE) strategy of modular multiple dual active bridge DC-DC converters for power sharing control," *2018 IEEE Energy Conversion Congress and Exposition (ECCE)*, 2018.
- [25] F. Xue, R. Yu, and A. Q. Huang, "A 98.3% efficient gan isolated bidirectional DC-DC converter for DC Microgrid Energy Storage System Applications," *IEEE Transactions on Industrial Electronics*, vol. 64, no. 11, pp. 9094-9103, 2017.
- [26] R. A. Abramson, S. J. Gunter, D. M. Otten, K. K. Afridi, and D. J. Perreault, "Design and evaluation of a reconfigurable stacked active bridge DC-DC converter for efficient wide load range operation," *IEEE Transactions on Power Electronics*, vol. 33, no. 12, pp. 10428-10448, 2018.
- [27] X. Zhang, L. Corradini, and D. Maksimovic, "Sensorless current sharing in digitally controlled Two-phase Buck DC-DC converters," *2009 Twenty-Fourth Annual IEEE Applied Power Electronics Conference and Exposition*, 2009.
- [28] P. Zumel, C. Fernández, A. de Castro and O. García, "Efficiency improvement in multiphase converter by changing dynamically the number of phases," *2006 37th IEEE Power Electronics Specialists Conference*, Jeju, Korea (South), 2006, pp. 1-6, doi: 10.1109/pesc.2006.1712202.
- [29] A. Kelly, "Current Share in Multiphase DC-DC Converters Using Digital Filtering Techniques," in *IEEE Transactions on Power Electronics*, vol. 24, no. 1, pp. 212-220, Jan. 2009, doi: 10.1109/TPEL.2008.2006752.
- [30] C. Liu, H. Liu, G. Cai, S. Cui, H. Liu and H. Yao, "Novel Hybrid LLC Resonant and DAB Linear DC-DC Converter: Average Model and Experimental Verification," in *IEEE Transactions on Industrial Electronics*, vol. 64, no. 9, pp. 6970-6978, Sept. 2017, doi: 10.1109/TIE.2017.2682784.
- [31] Z. Yan, Z. Weibo, and T. Guanghui, "A core loss calculation method for DC/DC power converters based on sinusoidal losses," *IEEE Transactions on Power Electronics*, vol. 38, no. 1, pp. 692-702, 2023.
- [32] P. Wang, X. Chen, C. Tong, P. Jia, and C. Wen, "Large- and small-signal average-value modeling of dual-active-bridge DC-DC converter with triple-phase-shift control," *IEEE Transactions on Power Electronics*, vol. 36, no. 8, pp. 9237-9250, 2021.
- [33] S. Wang, J. Liu, Z. Liu, T. Wu and B. Liu, "Efficiency-based optimization of steady-state operating points for parallel source converters in stand-alone power system," *2016 IEEE 8th International Power Electronics and Motion Control Conference (IPEMC-ECCE Asia)*, Hefei, China, 2016, pp. 163-170, doi: 10.1109/IPEMC.2016.7512280.
- [34] M. Shahjalal, M. R. Ahmed, H. Lu, C. Bailey, and A. J. Forsyth, "An analysis of the thermal interaction between components in power converter applications," *IEEE Transactions on Power Electronics*, vol. 35, no. 9, pp. 9082-9094, 2020.
- [35] N. Hou and Y. W. Li, "Overview and comparison of modulation and control strategies for a nonresonant single-phase dual-active-bridge DC-DC converter," *IEEE Transactions on Power Electronics*, vol. 35, no. 3, pp. 3148-3172, 2020.
- [36] F. Krismer and J. W. Kolar, "Efficiency-optimized high-current dual active bridge converter for Automotive Applications," *IEEE Transactions on Industrial Electronics*, vol. 59, no. 7, pp. 2745-2760, 2012.
- [37] H. Shi, H. Wen, Y. Hu, and L. Jiang, "Reactive power minimization in bidirectional DC-DC converters using a unified-phasor-based particle swarm optimization," *IEEE Transactions on Power Electronics*, vol. 33, no. 12, pp. 10990-11006, 2018.
- [38] J. Everts, "Closed-form solution for efficient ZVS modulation of DAB converters," *IEEE Transactions on Power Electronics*, vol. 32, no. 10, pp. 7561-7576, 2017.

- [39] N. Hou, W. Song, and M. Wu, "Minimum-current-stress scheme of Dual Active Bridge DC-DC converter with unified-phase-shift control," *IEEE Transactions on Power Electronics*, pp. 1–1, 2016.
- [40] S. Chaurasiya and B. Singh, "Performance of SPS control with external and internal phase shift for DAB DC-DC converter," *2020 IEEE International Conference on Computing, Power and Communication Technologies (GUCON)*, 2020.
- [41] H. Bai and C. Mi, "Eliminate Reactive Power and Increase System Efficiency of Isolated Bidirectional Dual-Active-Bridge DC-DC Converters Using Novel Dual-Phase-Shift Control," in *IEEE Transactions on Power Electronics*, vol. 23, no. 6, pp. 2905-2914, Nov. 2008, doi: 10.1109/TPEL.2008.2005103.